Acta Mech 219, 91–109 (2011)
DOI 10.1007/s00707-010-0438-y

Joel Jiménez-Lozano · Mihir Sen · Edmundo Corona

Analysis of peristaltic two-phase flow with application to ureteral biomechanics

Received: 19 May 2010 / Published online: 26 January 2011

Abstract Fluid flow in the ureter is sometimes accompanied by solid particles that are produced in the kidneys or result from the breakup of larger kidney stones; ureteral peristalsis is affected by the presence of these solids. Peristaltic flow is analyzed for a solitary traveling wave in an axisymmetric tube with an incompressible, Newtonian fluid in which identical, solid spherical particles are distributed. A two-phase flow model is used in conjunction with a perturbation method based on a small radius to length ratio of the wave to obtain a closed-form solution of the flow and particle velocities. The phenomenon of trapping in which closed fluid recirculation streamlines in a moving coordinate frame occurs is discussed. Peristaltic pumping is affected as particle volume fraction is increased. The pressure drop diminishes as the amplitude ratio (wave amplitude/wave radius) decreases. The pressure in the contracted part of the ureter increases as the particle volume fraction is increased. It is suggested that certain pathological and physiological manifestations on the ureter can be related to these findings. The results may also be relevant to the transport of other physiological fluids and industrial applications in which peristaltic pumping is used.

List of symbols

a	Particle radius
a_b	Wave amplitude
b	Characteristic length
c	Wave velocity
C	Volume fraction
H	Equation of wall in fixed frame
$\mathbf{M}$	Drag force per unit volume
p	Pressure
P	Pressure rise over characteristic length
q	Flow rate in moving frame
q_c	Critical flow rate for bifurcation in moving frame

J. Jiménez-Lozano · M. Sen (✉) · E. Corona
Department of Aerospace and Mechanical Engineering, University of Notre Dame, Notre Dame, IN 46556, USA
E-mail: Mihir.Sen.1@nd.edu

Present Address:
E. Corona
Sandia National Laboratories, Albuquerque, NM 87185, USA

q_λ	Flow rate characteristic value in moving frame
Q	Time-averaged flow rate in fixed frame
$\widehat{Q}$	Instantaneous flow rate in fixed frame
(r, z)	Spatial coordinates in moving frame
(R, Z)	Spatial coordinates in fixed frame
R_b	Wave radius
Re_0	Liquid Reynolds number
$\overline{Re}$	Modified Reynolds number
S	Stokes drag coefficient
t	Time
(u, v)	Axial and radial velocity in moving frame
(U, V)	Axial and radial velocity in fixed frame

Greek symbols

α	$= \rho_p/\rho_f$, Density ratio between phases
ϵ	$= R_b/b$, Nondimensional wave slope
η	Equation of wall in moving frame
λ	Axial length
μ	Viscosity
μ_0	Fluid viscosity
ρ	Density
$\boldsymbol{\tau}$	Viscous stress tensor
ϕ	$= a_b/R_b$, Amplitude ratio
ψ	Stream-function

Subscripts and superscripts

f	Fluid phase
p	Particle phase
r	Relative
s	Suspension
*	Dimensional quantities

1 Introduction

The term "peristalsis" is used for the mechanism by which a fluid can be transported through a distensible tube (or channel) when contraction or expansion waves propagate along its length. The literature on peristaltic flow is now quite extensive [1–12]. Early analyses of peristaltic motion were simplified by introducing approximations such as periodic, sinusoidal wave trains in infinitely long tubes or channels, small wall slopes, or low flow Reynolds number. The main objectives were to characterize the basic fluid mechanics of the process and, in particular, to find the pressure gradients that are generated by the wave, the flow behavior in the tube or channel due to peristalsis, and the conditions for trapping or reflux. Numerical methods have been employed to model peristalsis in a circular cylindrical tube at low Reynolds number and small slopes at the wall using finite differences [7], finite volumes [8], and in two-dimensional channels using a boundary integral method for Stokes flow [13]. Experimental studies of peristaltic flow include that by Yin and Fung [9] who studied a planar two-dimensional geometry and compared their results with an analytical solution; different reflux conditions were discussed. Graw and Engelhardt [14] set up an experimental facility to emulate ureteral peristalsis, and the influence of thickness and luminal position of the catheter on pressure measurements during peristaltic activity was investigated.

Physiological fluids in humans or animals are, in general, propelled by the continuous periodic muscular contraction or expansion (or both) of the ducts through which the fluid passes. In particular, peristaltic mechanisms may be involved in the swallowing of food through the esophagus, vasomotion of small blood vessels, spermatic flows in the ductus efferentes of the male reproductive tract, embryo transport in the uterus, and transport of urine through the ureter, among others.

In the esophageal deglutition, the larynx retrieves its normal position and the bolus is propelled into the esophagus by the contraction of the cricopharyngeus muscle. A peristaltic wave begins to propagate down the

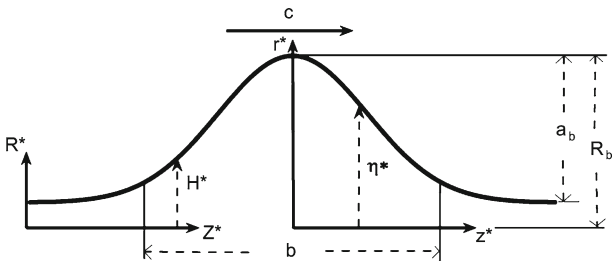

Fig. 1 Geometry of axisymmetric tube and bolus

esophagus carrying the bolus to the lower end where it is squeezed out into the cardiac sphincter [15]. Misra and Pandey [16] studied the flow of a food bolus through the esophagus by considering a model that involves the study of axisymmetric peristaltic transport of a power-law fluid. The effect of the nature of the wave and the power-law index on the pressure distribution along the esophagus was investigated. The vasomotion of small blood vessels, e.g., venules and arterioles, and the motion of lymphatic vessels have also been found to be peristaltic in nature [15]. In these vessels, smooth muscles in the wall exert a pumplike action by inherent rhythmical contractions, producing a one-way flow [17]. Mernone et al. [18] and Misra and Pandey [19] studied peristaltic blood flow in small vessels by considering a two-layer fluid model where the core region is a Casson model and the peripheral layer region is Newtonian viscous. The ductus efferentes (or vas deferens) is a long duct originating at the testis near the epidymis and joins the seminal vesicle to form the common ejaculatory duct. Gupta and Seshadri [20] analyzed peristaltic flow through non-uniform channels and tubes with particular reference to the flow of spermatic fluid in vas deferens, neglecting inertia terms. Peristalsis in reproduction is a central mechanism in embryo transport to an implantation in the uterus, and it contributes to ovum transport in the oviduct [21]. Eytan and Elad [22] studied the fluid-flow patterns in the uterus to understand embryo transport; intra-uterine fluid transport was simulated by a peristaltic transport lubrication model in a two-dimensional channel. Flow fields and possible trajectories of the embryo were provided.

The urinary system is responsible for the homeostatic regulation of water and ion content of blood and the disposal of waste products of metabolism. The kidneys receive blood from the renal artery, process it, and return the processed blood to the body through the renal vein. Urine produced in the kidneys passes through the ureters and is stored in the bladder that, by reflex action, contracts and expels urine through the urethra. The ureters are muscular tubes that can propel urine by peristalsis. They normally remain closed for much of the time, but every few seconds a wave of muscular contraction in the ureteral wall propels a bolus of urine from the kidney to the bladder. Lykoudis and Roos [5] studied the ureter fluid flow under a lubrication approximation and focused their analysis on the pressure profile in the contracted part. Griffiths [6] studied the ureter with a one-dimensional lubrication approach and emphasized the relation between low and high flow rates, pressure fields, and peristaltic contractions.

Although physiological fluid flows are similar with respect to peristalsis, their main differences lie in the fluid being transported, the geometry of the vessel or cavity, and the wave form. Both Newtonian and non-Newtonian fluids have been considered in ureteral, esophageal, and vasomotion peristalsis, e.g., Newtonian for urine, a power-law for the food bolus, and a Casson fluid for blood. Mostly, two-dimensional and axisymmetric geometries are studied, and a sinusoidal wave form is generally employed. The main motivation for any mathematical analysis of physiological fluid flows is to ultimately have a better understanding of the particular flow being modeled. Since there are some differences between peristalsis in different physiological systems, we have chosen to concentrate on the ureter. In this work, we will study ureteral peristalsis, extending Newtonian flow to particle-fluid mixtures.

It has been pointed out that peristalsis in the ureter occurs not as a sinusoidal but as a solitary wave [5], but this kind of wall motion has not been studied. A solitary peristaltic wave is shown in Fig. 1. The main parameters for the problem of peristaltic transport are the amplitude ratio $\phi \equiv a_b/R_b$ (which determines the relative degree of geometric occlusion), the wall slope $\epsilon \equiv R_b/b$, the Reynolds number Re (which is the ratio of inertial to viscous forces), and a pressure or flow rate condition. For the ureter, actual values of $(1-\phi)$ and ϵ seem to be very small. The presence of these small parameters enables asymptotic solutions to be obtained.

As mentioned, in ureteral peristalsis situations exist in which a single-phase medium is not a valid assumption since minerals sometimes precipitate in the kidneys to form small crystal matrices commonly called ureteral calculi or stones. Several methods have been developed to treat ureteral stones. A commonly used procedure is shock wave lithotripsy (SWL), in which an extracorporeal acoustic generator is used to break up

the stones into small pieces that are easier to transport along the ureter. Motivated by this, the purpose of the present work is to analyze peristaltic flow in the ureter due to a solitary wave with the objective of explaining the flow mechanics of a particle-fluid mixture.

Two-phase flows are also used in many industrial applications and have been widely studied. In addition, peristaltic pumps have been exploited for industrial applications like sanitary transport and the transport of corrosive fluids where contact of the fluid with machine parts is undesirable. A general classification of two-phase flows is that of Ishii and Hibiki [23], who divide them into four groups depending on the constituents of the flow: gas–solid, gas–liquid, solid–liquid, and flows of immiscible fluids. Here, we are interested in a dispersed solid–liquid flow, or particle–fluid mixture as the medium. The modeling of an isothermal two-phase flow problem using partial differential equations falls broadly into two categories: transport and two-fluid models. A transport model is formulated by considering the mixture as a whole and can be represented by one continuity, one momentum, and one diffusion equation to take into account the effect of volume fraction gradients. A two-fluid model consists of two continuity and two momentum equations [23–28]. This model is most appropriate if the dispersed particle phase behaves like a continuum, which is what is studied here. It is based on a macroscopic formulation with proper averaging. The general idea is to first formulate integral balances for mass and momentum for a fixed control volume containing both phases. This balance must be satisfied at any instant and location, resulting in two types of equations, one being the local instantaneous equations for each phase and the other an expression of the local instantaneous interfacial jump conditions. Numerical solutions can be obtained using different approaches. Enwald et al. [28] used a continuum–continuum approach (or Eulerian–Eulerian) in which the particle phase is considered to be a continuous fluid interpenetrating and interacting with the fluid phase. Patankar and Joseph [29] used an Eulerian–Lagrangian formulation where each computational parcel is considered to represent a group of particles interacting with the fluid and possessing the same characteristics of size and composition; positions of these parcels are then calculated using Newton's second law. Particle motion in peristaltic fluid flow has been studied in [30,31].

Numerical methods for the solutions of two-phase flow equations are widely used due to the complexity of the field equations. The calculated results, however, can depend on items such as the choice of a difference grid, the representation of differences on the grid, and the method of solving the difference equations [32]. In this work, we look for an analytical solution by taking advantage of approximations due to the existence of small parameters. A two-phase flow model that accounts for a mixture of dispersed small particles in a fluid as the working medium and that lends itself to analysis was presented by Drew [24–26]. It has been applied to peristaltic pumping [33–35] and is the model that will be used here.

The geometrical form of the peristaltic wave in the ureter is taken to be a solitary, axisymmetric wave. The governing equations are in the form of two continuity and two momentum equations, one each for the fluid and the particulate phase. A regular perturbation series in which the variables are expanded in a power series of wave slope ϵ is used to solve the problem. Closed form solutions up to order ϵ^2 are presented, and the influence of the particle volume fraction is investigated. The procedure of Lykoudis and Roos [5] is followed for the pressure profile.

2 Formulation of problem

The geometry of the problem is shown in Fig. 1, which is an instantaneous picture of a fluid bolus with a solitary wave moving along the walls of an axisymmetric tube in the axial direction at a speed c. The axial and radial coordinates in a frame fixed to the laboratory are Z^* and R^*. The deformation of the wall in this frame is assumed to be $H^*(Z^*, t^*) = R_b - a_b\left[1 - \exp\left\{-(Z^* - ct^*)^2/b^2\right\}\right]$, where t^* is time, a_b is the height of the wave, R_b is the radius at maximum height, and b is a characteristic length of the wave. The flow in the tube is unsteady in the fixed frame (Z^*, R^*), but becomes steady if a moving coordinate system (z^*, r^*) traveling at the speed of the wave is used. The coordinate frames are related by $z^* = Z^* - ct^*, r^* = R^*$, and the velocity components by $u^* = U^* - c, v^* = V^*$, where (U^*, V^*) and (u^*, v^*) are the axial and radial velocity components in the fixed and moving coordinate systems, respectively. The transformations are applied to the fluid (subscript f) and particle phase (subscript p) governing equations. The shape of the wall in the moving frame is then

$$\eta^*(z^*) = R_b - a_b\left\{1 - \exp\left(-\frac{z^{*2}}{b^2}\right)\right\}. \tag{1}$$

The steady-state governing equations, according to the two-phase model of Drew [24–26], are the conservation of mass and linear momentum equations

$$\nabla \cdot (1-C)\mathbf{v}_f^* = 0, \tag{2}$$

$$(1-C)\rho_f \left(\mathbf{v}_f^* \cdot \nabla \mathbf{v}_f^*\right) = -(1-C)\nabla p^* + \nabla \cdot (1-C)\boldsymbol{\tau}_f^* - \mathbf{M}_s^* \tag{3}$$

for the fluid and

$$\nabla \cdot C\mathbf{v}_p^* = 0, \tag{4}$$

$$C\rho_p \left(\mathbf{v}_p^* \cdot \nabla \mathbf{v}_p^*\right) = -C\nabla p^* + \mathbf{M}_s^* \tag{5}$$

for the particle phase. There is no viscous dissipation in the particle phase. The particle volume fraction gradient has been shown to be negligible [36] and is not included in the pressure terms in Eqs. (3) and (5). C is the volume fraction of particles, $\mathbf{v}_p^*$ is the particle velocity field, $\mathbf{v}_f^*$ is the fluid velocity field, p^* is the pressure, and ρ_f and ρ_p are the densities of the fluid and particle materials, respectively. It is assumed that the pressures in the two phases are equal [28,36]. The fluid is assumed to be incompressible and Newtonian, so the viscous stress tensor is of the form $\boldsymbol{\tau}_f^* = \mu_s\left(\nabla \mathbf{v}_f^* + (\nabla \mathbf{v}_f^*)^{\mathrm{T}}\right)$. The viscosity of the suspension, μ_s, depends on C. The fluid pressure gradient force is $-C\nabla p^*$. Momentum exchange is through a drag force per unit volume $\mathbf{M}_s^* = CS(\mathbf{v}_f^* - \mathbf{v}_p^*)$, where S is the Stokes drag coefficient between the phases. The assumptions are that the medium is dilute and dispersed, and that the Reynolds number is small, so that particle interaction forces, the virtual mass force (force exerted on a moving object when it accelerates), and the Faxén force (the viscous force derived from the curvature of the velocity field) [26,37,38] can be neglected.

For the fluid phase, the axisymmetric equations in cylindrical coordinates (z^*, r^*) are

$$\frac{1}{r^*}\frac{\partial}{\partial r^*}\left[(1-C)r^* v_f^*\right] + \frac{\partial}{\partial z^*}\left[(1-C)u_f^*\right] = 0, \tag{6}$$

$$\begin{aligned}(1-C)\rho_f\left(v_f^*\frac{\partial v_f^*}{\partial r^*} + u_f^*\frac{\partial v_f^*}{\partial z^*}\right) = &-(1-C)\frac{\partial p^*}{\partial r^*} + (1-C)\mu_s\left[\frac{\partial}{\partial r^*}\left(\frac{1}{r^*}\frac{\partial}{\partial r^*}\left(r^* v_f^*\right)\right) + \frac{\partial^2 v_f^*}{\partial z^{*2}}\right] \\ &+ 2\frac{\partial}{\partial r^*}\left((1-C)\mu_s\right)\frac{\partial v_f^*}{\partial r^*} + \frac{\partial}{\partial z^*}\left((1-C)\mu_s\right)\left(\frac{\partial u_f^*}{\partial r^*} + \frac{\partial v_f^*}{\partial z^*}\right) \\ &+ (1-C)\mu_s\frac{\partial^2 u_f^*}{\partial r^* \partial z^*} + CS(v_p^* - v_f^*),\end{aligned} \tag{7}$$

$$\begin{aligned}(1-C)\rho_f\left(v_f^*\frac{\partial u_f^*}{\partial r^*} + u_f^*\frac{\partial u_f^*}{\partial z^*}\right) = &-(1-C)\frac{\partial p^*}{\partial z^*} + (1-C)\mu_s\left[\frac{1}{r^*}\frac{\partial}{\partial r^*}\left(r^*\frac{\partial u_f^*}{\partial r^*}\right) + \frac{\partial^2 u_f^*}{\partial z^{*2}}\right] \\ &+ 2\frac{\partial}{\partial z^*}\left((1-C)\mu_s\right)\frac{\partial u_f^*}{\partial z^*} + \frac{\partial}{\partial r^*}\left((1-C)\mu_s\right)\left(\frac{\partial v_f^*}{\partial z^*} + \frac{\partial u_f^*}{\partial r^*}\right) \\ &+ (1-C)\mu_s\frac{1}{r^*}\frac{\partial}{\partial r^*}\left(r^*\frac{\partial v_f^*}{\partial z^*}\right) + CS(u_p^* - u_f^*).\end{aligned} \tag{8}$$

On the other hand, for the particle phase

$$\frac{1}{r^*}\frac{\partial}{\partial r^*}\left(Cr^* v_p^*\right) + \frac{\partial}{\partial z^*}\left(Cu_p^*\right) = 0, \tag{9}$$

$$C\rho_p\left(v_p^*\frac{\partial v_p^*}{\partial r^*} + u_p^*\frac{\partial v_p^*}{\partial z^*}\right) = -C\frac{\partial p^*}{\partial r^*} + CS(v_f^* - v_p^*), \tag{10}$$

$$C\rho_p\left(v_p^*\frac{\partial u_p^*}{\partial r^*} + u_p^*\frac{\partial u_p^*}{\partial z^*}\right) = -C\frac{\partial p^*}{\partial z^*} + CS(u_f^* - u_p^*). \tag{11}$$

Since C is the volume fraction of the particles in the mixture, $(1-C)\rho_f$ is the fluid phase density and $C\rho_p$ is the particle phase density.

The expression for the drag coefficient is $S = 9\mu_0/2a^2$, where μ_0 is the fluid viscosity and a is the particle radius. S represents the Stokes drag for a small particle and low Reynolds number. The presence of the dispersed particles in the suspension affects the mechanical properties of the averaged media. The way in which the moving parts of the fluid mixture interact among themselves and with solid walls is quantitatively different from the behavior of the pure fluid under similar circumstances. Several relations for the viscosity of a suspension as function of particle volume fraction and the viscosity of the suspending medium exist. For the particle-fluid mixture model, Srivastava and Srivastava [33] suggest the relation proposed by Charm and Kurland [39], which is, however, more appropriate for a blood suspension. For the present problem, the simplest form which is known as Einstein's formula, $\mu_s = \mu_0\,\mu_r$, will be used, where $\mu_r(C) = 1 + 5C/2$.

The dimensionless quantities $r \equiv r^*/R_b, z \equiv z^*/b, \eta \equiv \eta^*/R_b, u_f \equiv u_f^*/c, v_f \equiv v_f^*/\epsilon c, u_p \equiv u_p^*/c, v_p \equiv v_p^*/\epsilon c$, and $p \equiv p^*\epsilon R_b/\mu_s c$ are now introduced. Two geometrical dimensionless parameters present themselves in this formulation, ϕ and ϵ. The liquid Reynolds number may be defined as $Re_0 \equiv \rho_f R_b c/\mu_0$ and a modified Reynolds number as $\overline{Re} = \epsilon Re_0$. The drag parameter is $M \equiv (9/2)(R_b/a)^2$, where a is the particle radius. The density ratio between phases, $\alpha \equiv \rho_p/\rho_f$.

Equation (1) takes the form $\eta(z) = 1 - \phi\left\{1 - \exp\left(-z^2\right)\right\}$. The governing equations (6)–(11) become

$$\frac{1}{r}\frac{\partial}{\partial r}[(1-C)rv_f] + \frac{\partial}{\partial z}[(1-C)u_f] = 0, \tag{12}$$

$$\begin{aligned}\epsilon^3(1-C)Re_0\left(v_f\frac{\partial v_f}{\partial r} + u_f\frac{\partial v_f}{\partial z}\right) &= -\mu_r(1-C)\frac{\partial p}{\partial r} + \mu_r(1-C)\left[\epsilon^2\frac{\partial}{\partial r}\left(\frac{1}{r}\frac{\partial}{\partial r}(rv_f)\right) + \epsilon^4\frac{\partial^2 v_f}{\partial z^2}\right]\\ &\quad + 2\epsilon^2\frac{\partial}{\partial r}\left((1-C)\mu_r\right)\frac{\partial v_f}{\partial r} + \epsilon^2\frac{\partial}{\partial z}\left((1-C)\mu_r\right)\left(\frac{\partial u_f}{\partial r} + \epsilon^2\frac{\partial v_f}{\partial z}\right)\\ &\quad + \epsilon^2\mu_r(1-C)\frac{\partial^2 u_f}{\partial r\partial z} + \epsilon^2 MC(v_p - v_f),\end{aligned} \tag{13}$$

$$\begin{aligned}\epsilon(1-C)Re_0\left(v_f\frac{\partial u_f}{\partial r} + u_f\frac{\partial u_f}{\partial z}\right) &= -\mu_r(1-C)\frac{\partial p}{\partial z} + \mu_r(1-C)\left[\frac{1}{r}\frac{\partial}{\partial r}\left(r\frac{\partial u_f}{\partial r}\right) + \epsilon^2\frac{\partial^2 u_f}{\partial z^2}\right]\\ &\quad + 2\epsilon^2\frac{\partial}{\partial z}\left((1-C)\mu_r\right)\frac{\partial u_f}{\partial z} + \frac{\partial}{\partial r}\left((1-C)\mu_r\right)\left(\epsilon^2\frac{\partial v_f}{\partial z} + \frac{\partial u_f}{\partial r}\right)\\ &\quad + \epsilon^2\mu_r(1-C)\frac{1}{r}\frac{\partial}{\partial r}\left(r\frac{\partial v_f}{\partial z}\right) + MC(u_p - u_f),\end{aligned} \tag{14}$$

$$\frac{1}{r}\frac{\partial}{\partial r}\left(Crv_p\right) + \frac{\partial}{\partial z}\left(Cu_p\right) = 0, \tag{15}$$

$$\epsilon^3\alpha C Re_0\left(v_p\frac{\partial v_p}{\partial r} + u_p\frac{\partial v_p}{\partial z}\right) = -\mu_r C\frac{\partial p}{\partial r} + \epsilon^2 MC(v_f - v_p), \tag{16}$$

$$\epsilon\alpha C Re_0\left(v_p\frac{\partial u_p}{\partial r} + u_p\frac{\partial u_p}{\partial z}\right) = -\mu_r C\frac{\partial p}{\partial z} + MC(u_f - u_p). \tag{17}$$

The instantaneous volume flow rate of the suspension in the fixed (Z, R) coordinate system is given by $\widehat{Q}$, where $\widehat{Q} = \widehat{Q}_f + \widehat{Q}_p$; the instantaneous volume flow rate for the fluid and particle phases is given by $\widehat{Q}_f = 2\pi\int_0^H (1-C)U_f R\,\mathrm{d}R$ and $\widehat{Q}_p = 2\pi\int_0^H CU_p R\,\mathrm{d}R$. It must be mentioned that $\widehat{Q}_f = \widehat{Q}_f(Z,t)$, $\widehat{Q}_p = \widehat{Q}_p(Z,t)$, $H = H(Z,t)$, $U_f(Z,R,t)$, and $U_p(Z,R,t)$ are defined in the dimensionless fixed-frame coordinates (Z, R) with dimensionless time, $t = t^*/(b/c)$.

Using the relations between the fixed and the moving frame, $\widehat{Q} = q + \pi\eta^2$ is obtained, where q is the instantaneous volume flow rate in the moving coordinate system (z, r) and is independent of time. The time-average flow rate at each cross-section, $Q(Z)$, over an interval T at a fixed Z-position is [1,40]

$$\begin{aligned}Q &\equiv \frac{1}{T}\int_0^T \widehat{Q}\,\mathrm{d}t\\ &= q + \pi\Gamma,\end{aligned} \tag{18}$$

where $\Gamma = (1/T)\int_0^T \eta^2\,\mathrm{d}t$. The instantaneous volume flow rate in the moving frame, q, is given by $q = q_f + q_p$. The volume flow rates for the fluid phase, q_f, and the particulate phase, q_p, are given by $q_f = 2\pi\int_0^\eta (1-C)\,u_f r\,\mathrm{d}r$ and $q_p = 2\pi\int_0^\eta C u_p r\,\mathrm{d}r$.

For the fluid, the dimensionless boundary conditions are symmetric along the longitudinal axis and no slip-condition at the wall [1,5,40]. For the particles, only symmetry is assumed. These boundary conditions are

$$\begin{aligned}\frac{\partial u_f}{\partial r} &= 0 \text{ at } r = 0,\\ u_f &= -1 \text{ at } r = \eta(z),\\ \frac{\partial u_p}{\partial r} &= 0 \text{ at } r = 0.\end{aligned}$$

In an adult human, typical ureteral dimensions and bolus velocity, as suggested for biomechanical modeling by Boyarski et al. [41], are of the order of $R_b = 1.5\,\mathrm{mm}$, $b = 120\,\mathrm{mm}$, and $c = 27\,\mathrm{mm/s}$. Urine characteristics are similar to that of water so that the viscosity $\mu_0 = 0.00089\,\mathrm{Ns/m^2}$ at 298 K. For $C = 0$, using these values gives $\overline{Re} = 0.56$, indicating that viscous forces dominate over inertial forces. An approximate value for the wave slope is $\epsilon = 0.0125$, while the amplitude ratio is $0 < \phi < 1$. The particle size for dilute urine suspensions of renal calcium oxalate calculi is of the order $a = 10\,\mu\mathrm{m}$, as reported by Guerra et al. [42], so that a/R_b is of the order of $1/150$.

3 Perturbation solution

A regular perturbation expansion is used to solve the problem. It is assumed that the particle volume fraction C is low and that it can be considered constant of the form $C = \epsilon C^{(1)}$. Also, the solutions for the fluid, (u_f, v_f), particle velocities, (u_p, v_p), and pressure, p, are of the form

$$u_f(r,z;\epsilon) = {u_f}^{(0)} + \epsilon {u_f}^{(1)} + \epsilon^2 {u_f}^{(2)} + \cdots, \tag{19}$$

$$v_f(r,z;\epsilon) = {v_f}^{(0)} + \epsilon {v_f}^{(1)} + \epsilon^2 {v_f}^{(2)} + \cdots, \tag{20}$$

$$u_p(r,z;\epsilon) = {u_p}^{(0)} + \epsilon {u_p}^{(1)} + \epsilon^2 {u_p}^{(2)} + \cdots, \tag{21}$$

$$v_p(r,z;\epsilon) = {v_p}^{(0)} + \epsilon {v_p}^{(1)} + \epsilon^2 {v_p}^{(2)} + \cdots, \tag{22}$$

$$p(r,z;\epsilon) = p^{(0)} + \epsilon p^{(1)} + \epsilon^2 p^{(2)} + \cdots. \tag{23}$$

The small-wave slope or long-wave approximation, $\epsilon \ll 1$, is introduced. Substituting expansions in the governing equations, (12)–(17), and collecting terms of like powers of ϵ, the equations are reduced to a set of linear equations as shown next.

The zeroth-order system is given by

$$\frac{1}{r}\frac{\partial}{\partial r}[r{v_f}^{(0)}] + \frac{\partial}{\partial z}[{u_f}^{(0)}] = 0, \tag{24}$$

$$\frac{\partial p^{(0)}}{\partial r} = 0, \tag{25}$$

$$\frac{\partial p^{(0)}}{\partial z} = \frac{1}{r}\frac{\partial}{\partial r}\left(r\frac{\partial {u_f}^{(0)}}{\partial r}\right), \tag{26}$$

with the boundary conditions

$$\begin{aligned}\frac{\partial u_f^{(0)}}{\partial r} &= 0 \text{ at } r = 0,\\ u_f^{(0)} &= -1 \text{ at } r = \eta(z).\end{aligned}$$

The first-order system is given by

$$\frac{1}{r}\frac{\partial}{\partial r}[r{v_f}^{(1)}] + \frac{\partial}{\partial z}[{u_f}^{(1)}] = 0, \tag{27}$$

$$\frac{\partial p^{(1)}}{\partial r} + \frac{3}{2}C^{(0)}\frac{\partial p^{(0)}}{\partial r} = 0, \tag{28}$$

$$Re_0\left({v_f}^{(0)}\frac{\partial {u_f}^{(0)}}{\partial r} + {u_f}^{(0)}\frac{\partial {u_f}^{(0)}}{\partial z}\right) = -\frac{\partial p^{(1)}}{\partial z} - \frac{3}{2}C^{(1)}\frac{\partial p^{(0)}}{\partial z} + \frac{1}{r}\frac{\partial}{\partial r}\left(r\frac{\partial {u_f}^{(1)}}{\partial r}\right) + \frac{3}{2}C^{(1)}\frac{1}{r}\frac{\partial}{\partial r}\left(r\frac{\partial {u_f}^{(0)}}{\partial r}\right) + MC^{(1)}({u_p}^{(0)} - {u_f}^{(0)}), \tag{29}$$

$$C^{(1)}\left(\frac{1}{r}\frac{\partial}{\partial r}[r{v_p}^{(0)}] + \frac{\partial}{\partial z}[{u_p}^{(0)}]\right) = 0, \tag{30}$$

$$C^{(1)}\frac{\partial p^{(0)}}{\partial r} = 0, \tag{31}$$

$$C^{(1)}\frac{\partial p^{(0)}}{\partial z} = MC^{(1)}({u_f}^{(0)} - {u_p}^{(0)}), \tag{32}$$

with boundary conditions

$$\frac{\partial u_f^{(1)}}{\partial r} = 0 \text{ at } r = 0,$$
$$u_f^{(1)} = 0 \text{ at } r = \eta(z),$$
$$\frac{\partial u_p^{(0)}}{\partial r} = 0 \text{ at } r = 0.$$

The second-order system is given by

$$\frac{1}{r}\frac{\partial}{\partial r}[r{v_f}^{(2)}] + \frac{\partial}{\partial z}[{u_f}^{(2)}] = 0, \tag{33}$$

$$\frac{\partial p^{(2)}}{\partial r} + \frac{3}{2}C^{(1)}\frac{\partial p^{(1)}}{\partial r} - \frac{5}{2}{C^{(1)}}^2\frac{\partial p^{(1)}}{\partial r} = 0, \tag{34}$$

$$Re_0\left({v_f}^{(0)}\frac{\partial {u_f}^{(1)}}{\partial r} + {u_f}^{(0)}\frac{\partial {u_f}^{(1)}}{\partial z} + {v_f}^{(1)}\frac{\partial {u_f}^{(0)}}{\partial r} + {u_f}^{(1)}\frac{\partial {u_f}^{(0)}}{\partial z} - C^{(1)}\left({v_f}^{(0)}\frac{\partial {u_f}^{(0)}}{\partial r} + {u_f}^{(0)}\frac{\partial {u_f}^{(0)}}{\partial z}\right)\right)$$
$$= -\frac{\partial p^{(2)}}{\partial z} - \frac{3}{2}C^{(1)}\frac{\partial p^{(1)}}{\partial z} + \frac{5}{2}{C^{(1)}}^2\frac{\partial p^{(0)}}{\partial z} + \frac{1}{r}\frac{\partial}{\partial r}\left(r\frac{\partial {u_f}^{(2)}}{\partial r}\right) - \frac{5}{2}{C^{(1)}}^2\frac{1}{r}\frac{\partial}{\partial r}\left(r\frac{\partial {u_f}^{(0)}}{\partial r}\right)$$
$$+ \frac{3}{2}C^{(1)}\frac{1}{r}\frac{\partial}{\partial r}\left(r\frac{\partial {u_f}^{(1)}}{\partial r}\right) + MC^{(1)}({u_p}^{(1)} - {u_f}^{(1)}), \tag{35}$$

$$C^{(1)}\left(\frac{1}{r}\frac{\partial}{\partial r}[r{v_p}^{(1)}] + \frac{\partial}{\partial z}[{u_p}^{(1)}]\right) = 0, \tag{36}$$

$$C^{(1)}\frac{\partial p^{(1)}}{\partial r} + \frac{5}{2}{C^{(1)}}^2\frac{\partial p^{(0)}}{\partial r} = 0, \tag{37}$$

$$\alpha Re_0 C^{(1)}\left({v_p}^{(0)}\frac{\partial {u_p}^{(0)}}{\partial r} + {u_p}^{(0)}\frac{\partial {u_p}^{(0)}}{\partial z}\right) = -C^{(1)}\frac{\partial p^{(1)}}{\partial z} - \frac{5}{2}{C^{(1)}}^2\frac{\partial p^{(0)}}{\partial z} + MC^{(1)}({u_f}^{(1)} - {u_p}^{(1)}), \tag{38}$$

with boundary conditions

$$\frac{\partial u_f^{(2)}}{\partial r} = 0 \text{ at } r = 0,$$
$$u_f^{(2)} = 0 \text{ at } r = \eta(z),$$
$$\frac{\partial u_p^{(1)}}{\partial r} = 0 \text{ at } r = 0.$$

The system of equations (33)–(38) is solved order by order as shown in Appendix A. The calculations are expressed up to second order of the total flow rate in the moving frame, q, as $q \equiv q^{(0)} + \epsilon q^{(1)} + \epsilon^2 q^{(2)}$. Then, substituting $q^{(0)} = q - \epsilon q^{(1)} - \epsilon^2 q^{(2)}$ into the assembled solutions, Eqs. (19)–(23), and retaining terms to the second order in ϵ, a closed-form solution in terms of the total flow rate is obtained.

4 Results and discussion

The results of our analysis are presented as follows: (1) the streamlines, velocity profiles, and trapping regions for the parameters: $\{\phi;\ \epsilon;\ Re_0;\ C;\ q\}$ for the pure fluid, $C = 0$; (2) the pressure drop flow rate relations for the parameters: $\{\phi;\ \epsilon;\ Re_0;\ \alpha;\ a/R_b\}$; (3) the effect of C on the ureteral pressure profile in the contracted part compared with Lykoudis and Roos [5]. Though it is not possible to put $\phi = 1$ because of a mathematical singularity, it is easy to get as close to unity as needed.

4.1 Streamlines and velocity profiles

An important characteristic of peristaltic flow is that for certain parameter values regions exist where the streamlines are closed and the fluid recirculates, a phenomenon known as trapping. Streamlines in the moving frame with $\{\phi = 0.9;\ \epsilon = 0.0125;\ Re_0 = 50;\ C = 0\}$ are shown in Fig. 2a–d for different values of q. For very negative q, the fluid streamlines are generally similar to the shape of the wall, but with decreasing amplitude as the axis is approached, as shown in Fig. 2a. An interesting situation occurs on increasing q when, at a certain q, there is a bifurcation and the center streamline splits to enclose a ring-shaped bolus of fluid with closed streamlines. This bolus is centered under the crest as shown in Fig. 2b, and there are two stagnation points created at the axis. As q is further increased, the stagnation points move away from each other, as in Fig. 2c. The width of the trapped eddy measured at the centerline is larger for Fig. 2c than for Fig. 2b, so that as q increases its width does as well. Thus, the sequence of Fig. 2a–c shows that increasing the value of q leads to greater trapping. On further increasing q, the pattern changes again, as in Fig. 2d. This qualitative behavior concurs with the results of Siddiqui and Schwarz [40] and Mekheimer et al. [34]. Figure 3a–d show the longitudinal velocity profiles in the moving frame at various sections.

The velocity profile under the wave crest shows a point of zero-velocity when trapping occurs. This characteristic of the flow can be investigated using $u_f(z = 0, r) = 0$. Regimes of trapping can be investigated. In Fig. 4, a bifurcation diagram is traced for this point of zero-velocity in a $q - r$ plane for $Re_0 = 0$ for convenience, and it is compared with curves of different particle volume fraction. A critical flow rate, q_c, where the bifurcation occurs is shown in the bifurcation diagram; this critical flow rate is traced for different values of C and shown in Fig. 5. The effect of increasing the particle volume fraction is to diminish the value of the critical flow rate. Three different flow situations are manifested in peristaltic flow: backward, trapping, and augmented flow. The dynamics of the critical points (stagnation points) is rich. Modifications in parameter values produce changes in their stability and position. Topological changes in the flow patterns occur due to the creation and coalescence of critical points. A detailed analysis of streamline patterns and their local and global bifurcations in a two-dimensional planar and axisymmetric peristaltic flow for an incompressible Newtonian fluid have been previously presented [43].

4.2 Pressure drop flow rate relations

As the flow is steady in the moving frame, one can characterize the pumping performance by means of the pressure rise over a characteristic axial length. This can be defined as $\Delta P = \int_{-1}^{1} (dp/dz)\, dz$. Since dp/dz

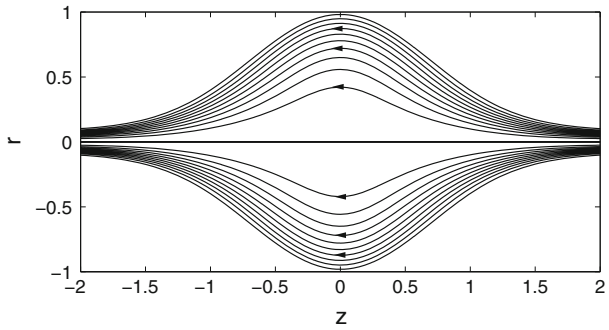

(a) $q = -2$ $(Q = -0.024)$

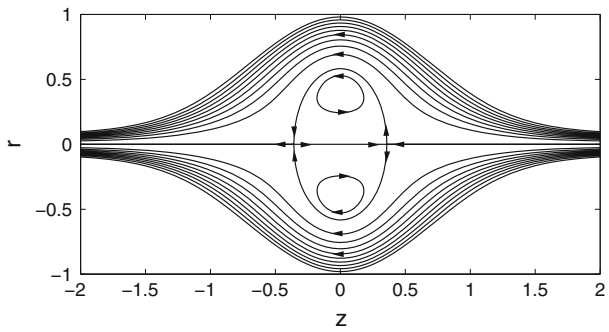

(b) $q = -1.25$ $(Q = 0.725)$

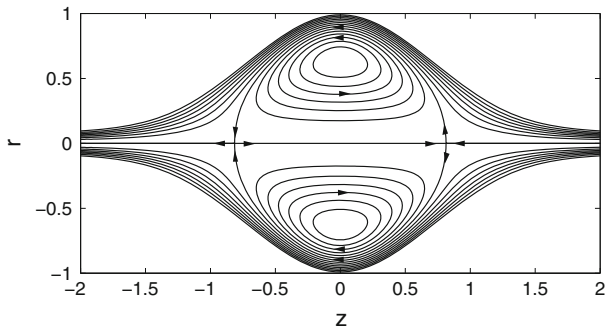

(c) $q = -0.5$ $(Q = 1.475)$

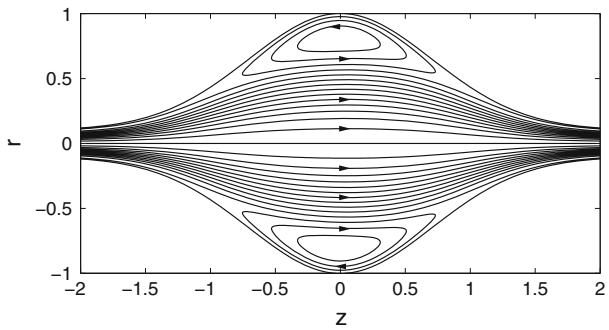

(d) $q = 1.5$ $(Q = 3.475)$

Fig. 2 Fluid streamlines in moving frame for different values of q with $\epsilon = 0.0125$, $\phi = 0.9$, $Re_0 = 50$, and $C = 0$

is independent of r, the integral can be evaluated at the axis at $r = 0$. The solutions for the pressure gradient $\mathrm{d}p^{(0)}/\mathrm{d}z$, $\mathrm{d}p^{(1)}/\mathrm{d}z$, and $\mathrm{d}p^{(2)}/\mathrm{d}z$ in terms of the flow rate are shown in Eqs. (43), (48), and (53). Now, $\Delta P = \Delta P^{(0)} + \epsilon \Delta P^{(1)} + \epsilon^2 \Delta P^{(2)} + \cdots$. The calculations are expressed up to second order of the total

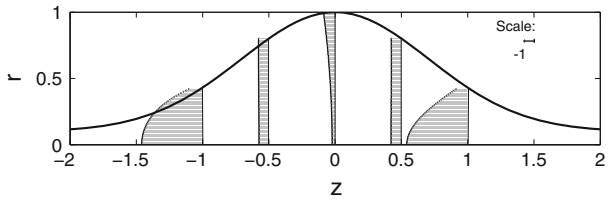

(a) $q = -2$ $(Q = -0.024)$

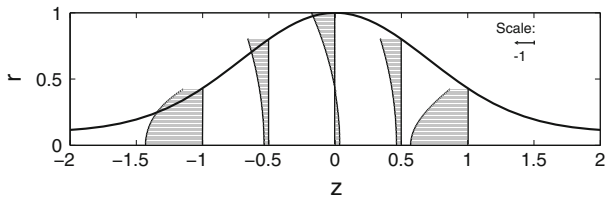

(b) $q = -1.25$ $(Q = 0.725)$

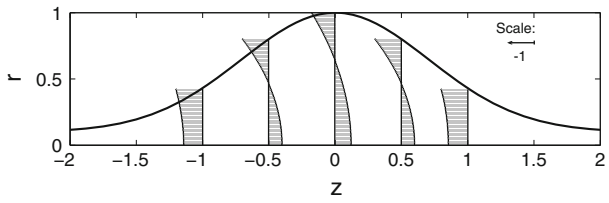

(c) $q = -0.5$ $(Q = 1.475)$

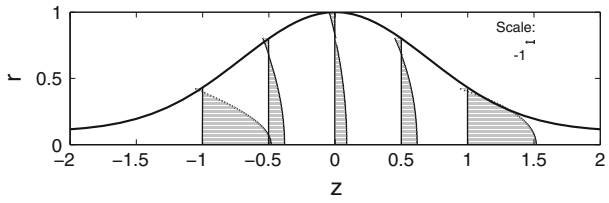

(d) $q = 1.5$ $(Q = 3.475)$

Fig. 3 Fluid longitudinal velocity profiles in moving frame for different values of q with $\epsilon = 0.0125$, $\phi = 0.9$, $Re_0 = 50$, and $C = 0$

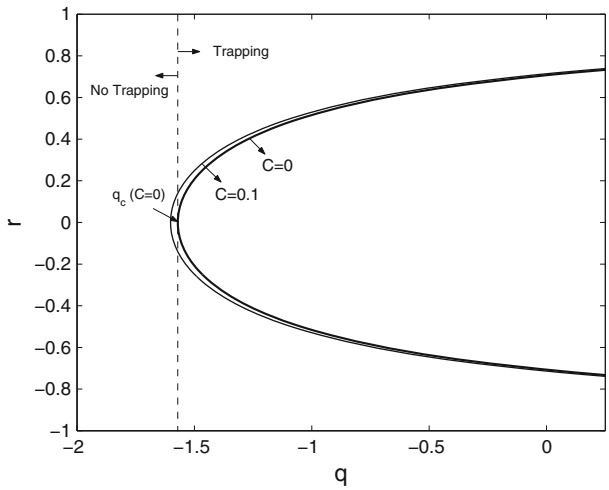

Fig. 4 Bifurcations of fixed point inside bolus with $Re_0 = 0$, $\phi = 0.9$, $a/R_b = 1/150$ for different values of C

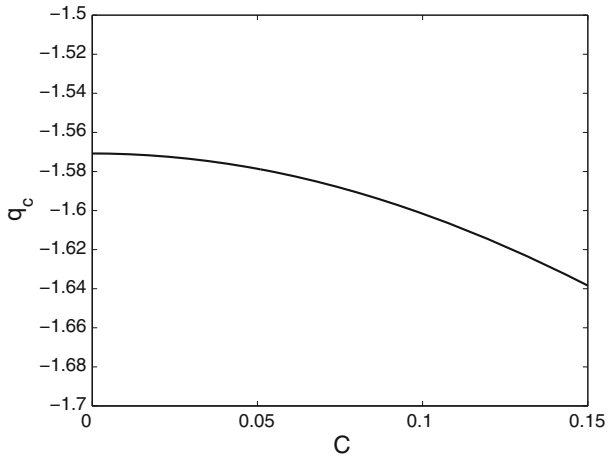

Fig. 5 Effect of particle volume fraction C on critical flow rate q_c where bifurcation occurs, with $Re_0 = 0$, $\phi = 0.9$ and $a/R_b = 1/150$

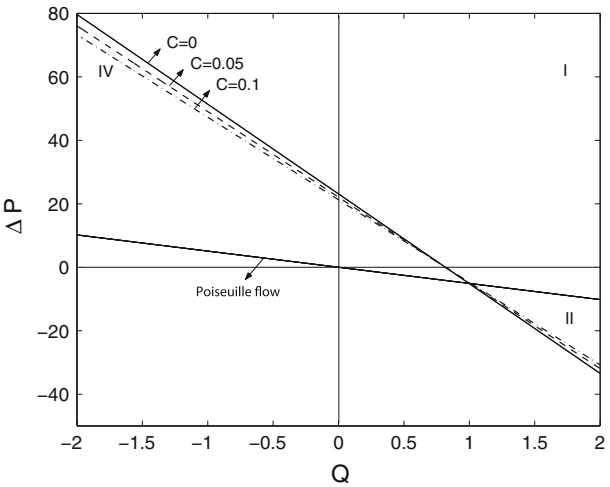

Fig. 6 Pumping characteristics for $C = 0$ (*solid line*); $C = 0.05$ (*dashed line*); $C = 0.1$ (*solid line with dot*); with $\phi = 0.9$, $\epsilon = 0.0125$, $Re_0 = 50$, $\alpha = 2$, $a/R_b = 1/150$, and Poiseuille flow ($\phi = 0$)

flow rate at the moving frame, q, as $q \equiv q^{(0)} + \epsilon q^{(1)} + \epsilon^2 q^{(2)}$. q and ΔP can be related by substituting $q^{(0)} = q - \epsilon q^{(1)} - \epsilon^2 q^{(2)}$ into the ΔP equation, integrating for each order, and retaining terms to the second order in ϵ.

The relation between ΔP and Q can be explored using Eq. (18). In Fig. 6, ΔP vs. Q is plotted for $\{\phi = 0.9;\ \epsilon = 0.0125;\ Re_0 = 50;\ \alpha = 2;\ a/R_b = 1/150\}$ for different values of C. The graph is sectored, so that quadrant *I* denotes the region of peristaltic pumping, where $Q > 0$ (positive pumping) and $\Delta P > 0$ (adverse pressure gradient). Quadrant *II*, where $\Delta P < 0$ (favorable pressure gradient) and $Q > 0$ (positive pumping), is augmented flow. Quadrant *IV*, in which $\Delta P > 0$ (adverse pressure gradient) and $Q < 0$, is backward pumping [40]. Also, these relations are compared with the classical Poiseuille flow.

For the upper half-plane in Fig. 6, there is an adverse pressure gradient acting against the peristalsis; it is observed that an increase in C results in a decrease in the pumping rate if all other parameters are held fixed. The backward pumping also increases with increase in particle volume fraction. In contrast, in the lower half-plane, there is a favorable pressure gradient acting in the same direction as peristalsis, and this enhances the transport of the particulate suspension.

It is observed from Figs. 6 and 7 that ΔP is higher for $\phi = 0.9$ compared with $\phi = 0.8$. Also, the pumping rate for zero pressure rise $Q(\Delta P = 0)$ decreases as ϕ is diminished. Note that $\phi = 1$ corresponds to a totally occluded bolus at the ends; $\phi \to 0$ can be seen as a dilatation of the ureter. In medical pathology, a dilatation from its normal size is treated as a disease, and it is known that dilated ureters compromise effective peristalsis

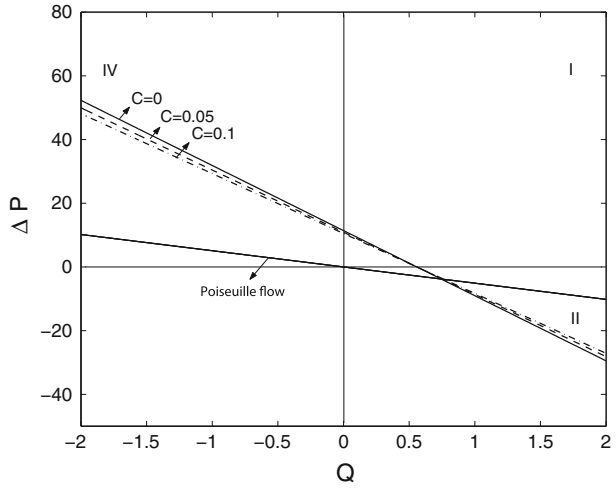

Fig. 7 Pumping characteristics for $C = 0$ (*solid line*); $C = 0.05$ (*dashed line*); $C = 0.1$ (*solid line with dot*); with $\phi = 0.8$, $\epsilon = 0.0125$, $Re_0 = 45$, $\alpha = 2$, $a/R_b = 1/150$ and Poiseuille flow ($\phi = 0$)

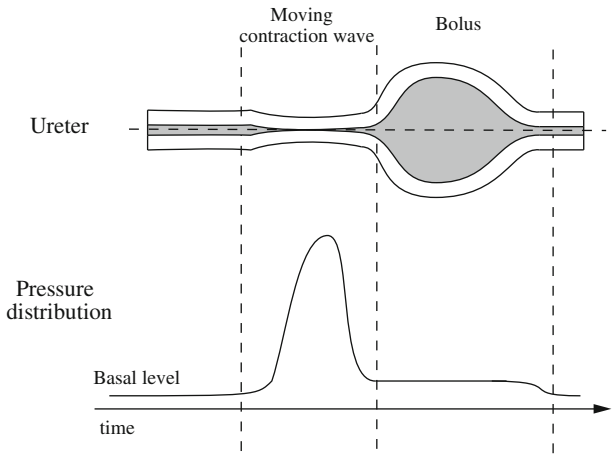

Fig. 8 Pressure distribution during passage of bolus through ureter

causing a deficiency of the bolus propulsion which eventually affects normal renal function (e.g., megaureter, hydronephrotic pelvis). The findings here also confirm that dilatation affects peristaltic pumping.

As mentioned before, an increase in C while maintaining the other parameters fixed diminishes the pumping rate in region I. So, peristaltic pumping is affected by the presence of the particles. For ureteral peristalsis, the presence of particulates in the suspension can affect its "normal" functioning. Moreover, it is known that with the existence of residual fragments after lithotripsy, these fragments can regrow in size and form new stones [44]. The present study points to the importance of clearing residuals and preventing regrowth.

4.3 Ureteral pressure profile

4.3.1 Solitary wave

Observations of ureteral peristalsis suggest that muscular activity creates a contraction wave that propels the bolus of urine along the ureter. During the passage of this bolus, the pressure reaches a maximum and decays to the basal level as shown in Fig. 8 (adapted from [6]). Kiil [45] first measured pressure in the ureter to understand its physiological functions, and several manometric studies have been reported since then [46–49]. In general, pressure measurements have been taken using pressure transducers attached to catheters inserted into the ureter and recording pressure histories (e.g., urometrogram, ureteric profilometry).

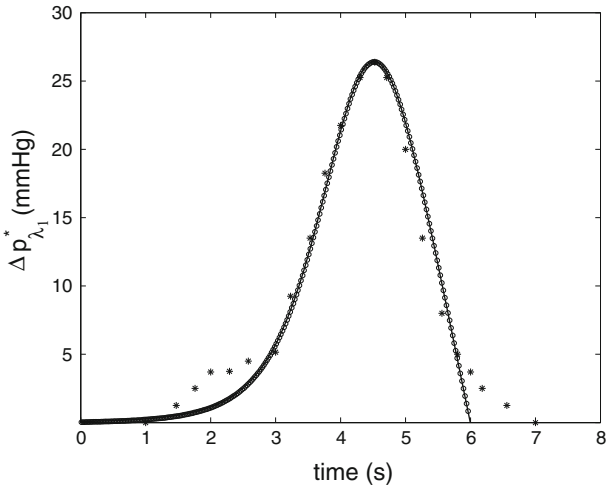

Fig. 9 Pressure distribution in contraction section; $a_1 = 2.35\,\text{mm}$, $b_1 = 0.02\,\text{mm}$, $c = 30\,\text{mm/s}$, $\lambda_1 = 250\,\text{mm}$; analytical (present theory, $C = 0$) *circle*; analytical (Lykoudis, Eq. (25)) *solid line*; experimental (Kiil, p. 59) *asterisk*

Lykoudis and Roos [5] investigated the fluid mechanics of the ureter using a wall profile different from the one used here and determined its relation to the urometrogam. Good agreement between the theoretical results using a lubrication approach ($\overline{Re} = 0$) and experimental pressure distributions was reported. The results of the present analysis for $\overline{Re} = 0$ are used for comparison purposes. The pressure gradient is given by

$$\frac{\mathrm{d}p}{\mathrm{d}z} = \frac{q}{\pi}\left(\frac{d_1}{\eta^4} + \frac{d_2}{\eta^6} + \frac{d_3}{\eta^8}\right) + \frac{d_1}{\eta^2} + \frac{d_2}{\eta^4} + \frac{d_3}{\eta^6}, \tag{39}$$

where $d_1 = -8(1 - C + 2C^2)$, $d_2 = 32(C^2 + 2C)/M$ and $d_3 = -(512C^2)/M^2$. This gives the local pressure gradient $\mathrm{d}p/\mathrm{d}z$ in terms of q, and this relation must be inverted to find q for a given $\mathrm{d}p/\mathrm{d}z$.

Uremetrograms suggest [45,48] that there does not exist an overall pressure gradient over one wavelength for the normal ureter. In such a case, it can be assumed that the gradient is zero over a wavelength. This assumption enables the pressure distribution to be determined. Thus,

$$\Delta p = p_{\lambda/2} - p_{-\lambda/2} = \int_{-\lambda/2}^{\lambda/2} \frac{\mathrm{d}p}{\mathrm{d}z}\,\mathrm{d}z = 0.$$

Upon integrating Eq. (39) over a period from $z = -\lambda/2$ to $z = \lambda/2$, the left-hand side vanishes, and the result can be rearranged to yield a characteristic value q_λ of q, which is given by

$$q_\lambda = -\pi\,\frac{\displaystyle\int_{-\lambda/2}^{\lambda/2}\left(\frac{d_1}{\eta^2} + \frac{d_2}{\eta^4} + \frac{d_3}{\eta^6}\right)\mathrm{d}z}{\displaystyle\int_{-\lambda/2}^{\lambda/2}\left(\frac{d_1}{\eta^4} + \frac{d_2}{\eta^6} + \frac{d_3}{\eta^8}\right)\mathrm{d}z}. \tag{40}$$

4.3.2 Comparison with Lykoudis and Roos

In this section, we temporarily go back to dimensional variables and assume that the geometry of the boundary near the contraction section is given as in [5]: $\eta_1^* = b_1 + a_1(z^*/\lambda_1)^4$, where $R_b = a_1 + b_1$ and $-\lambda_1 < z^* < 0$. Therefore, the pressure distribution in this part of the ureter can be estimated by $\Delta p_{\lambda_1}^* = \mu_s\left(q_{\lambda_1}^* I_1^* + \pi c I_2^*\right)/\pi$, where $I_1^* = \int_{-\lambda_1}^0 \left(\frac{d_1}{\eta_1^{*4}} + \frac{d_2}{\eta_1^{*6}} + \frac{d_3}{\eta_1^{*8}}\right)\mathrm{d}z^*$ and $I_2^* = \int_{-\lambda_1}^0 \left(\frac{d_1}{\eta_1^{*2}} + \frac{d_2}{\eta_1^{*4}} + \frac{d_3}{\eta_1^{*6}}\right)\mathrm{d}z$.

In Fig. 9, the result for the pressure distribution for the pure fluid with $C = 0$ is compared with that obtained in [5] under the lubrication approximation. The experimental values [45] are also included in the figure for

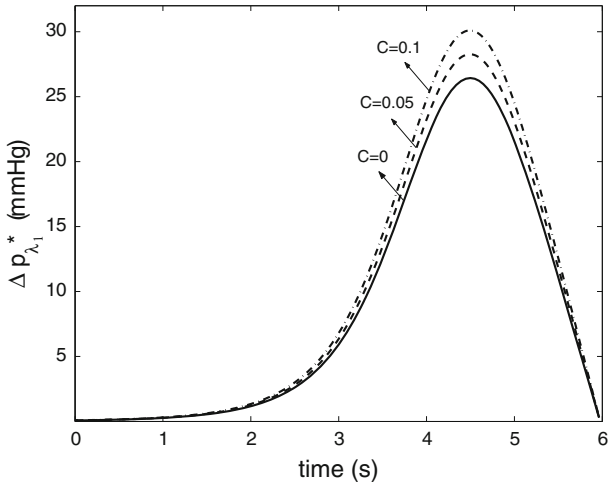

Fig. 10 Pressure distribution for $C = 0$ *solid line*; $C = 0.05$ *dashed line*; $C = 0.1$ *solid line with dot*; with $a_1 = 2.35\,\text{mm}$, $b_1 = 0.02\,\text{mm}$, $c = 30\,\text{mm/s}$, and $\lambda_1 = 250\,\text{mm}$

comparison. The maximum pressure occurs in the contracted part; this happens in a way similar to lubrication in thin films, so that the film of urine around the catheter behaves like a thin layer of fluid capable of sustaining high pressures.

The effect of the volume fraction of the particles is shown in Fig. 10. The pressure profile increases with C. This growth is related to an increase in the relative viscosity of the medium when particles are present. As an application, if one takes a normal uremetrogram of a patient before SWL treatment and compares it with the post-treatment uremetrogram, our analysis shows that there should be differences that indicate that residuals have not been completely cleared.

5 Conclusions

An analysis of axisymmetric peristaltic flow of a solid–liquid mixture in the ureter has been presented. The results can help understand the mechanics of ureteral peristalsis in the presence of solid particles, as in ureteral lithiasis.

The influence of the principal parameters, ϵ, ϕ, Re_0, q, a/R_b, α, and C, on the flow were examined. From an analysis of the streamlines and velocity profiles, it was found that on increasing q, the volume of trapped fluid increases if trapping is already present. There exists a critical flow rate in which the flow field topology changes from backward flow to trapping. The effect of increasing the volume fraction is to diminish the critical flow rate where bifurcation occurs. It is noted that even with an adverse pressure gradient, peristalsis contributes to positive pumping. The peristaltic pumping rate is diminished as particle volume fraction is increased; dispersed small particles immersed in the fluid medium affect the peristalsis. The pressure profile and the influence on it of the parameters were studied. As the particle volume fraction increases, the pressure profile increases as well.

Acknowledgments J.J.-L. is grateful for a Fellowship from the National Council for Science and Technology of México (CONACyT).

Appendix

A Zeroth-, First-, and Second-order Solutions

The zeroth-order system, Eqs. (24)–(26), is solved as follows. Eq. (25) implies that $p^{(0)} = f(z)$ only. Then, Eq. (26) is integrated to find $u_f^{(0)}$. The vertical velocity $v_f^{(0)}$ is calculated by integration of the continuity

equation, Eq. (24). The solution is closed by prescribing a known pressure gradient or a flow rate condition, and we are interested in the latter. The total flow rate at the zeroth order is $q^{(0)} = q_f^{(0)} + q_p^{(0)}$, where $q_f^{(0)} = 2\pi \int_0^\eta u_f^{(0)} r \, \mathrm{d}r$ and $q_p^{(0)} = 0$.
The solution at the zeroth order is

$$u_f^{(0)} = \frac{1}{4}\frac{\mathrm{d}p^{(0)}}{\mathrm{d}z}\left(r^2 - \eta^2\right) - 1, \tag{41}$$

$$v_f^{(0)} = \frac{\mathrm{d}p^{(0)}}{\mathrm{d}z}\frac{\eta\eta'}{4}r - \frac{1}{16}\left(\frac{\mathrm{d}p^{(0)}}{\mathrm{d}z}\right)'\left(r^3 - 2\eta^2 r\right), \tag{42}$$

$$\frac{\mathrm{d}p^{(0)}}{\mathrm{d}z} \equiv K_0 = -\frac{8}{\pi}\left[\frac{q^{(0)} + \pi\eta^2}{\eta^4}\right]. \tag{43}$$

The system Eqs. (27)–(32) is solved similarly. Note that the total flow rate at the first order is $q^{(1)} = q_f^{(1)} + q_p^{(1)}$, where $q_f^{(1)} = 2\pi \int_0^\eta u_f^{(1)} r \mathrm{d}r - 2\pi C^{(1)} \int_0^\eta u_f^{(0)} r \mathrm{d}r$ and $q_p^{(1)} = 2\pi C^{(1)} \int_0^\eta u_p^{(0)} r \mathrm{d}r$.
The solution at the first order is given by

$$u_f^{(1)} = \frac{a_1}{36}\left(r^6 - \eta^6\right) + \frac{a_2}{16}\left(r^4 - \eta^4\right) + \left[\frac{a_3 + K_1 + C^{(1)}K_0}{4}\right]\left(r^2 - \eta^2\right), \tag{44}$$

$$\begin{aligned} v_f^{(1)} = {} & -\frac{a_1{}'}{288}(r^7 - 4\eta^6 r) - \frac{a_2{}'}{96}(r^5 - 3\eta^4 r) - \frac{a_3{}'}{16}(r^3 - 2\eta^2 r) + \frac{a_1}{12}\eta^5\eta' r + \frac{a_2}{8}\eta^3\eta' r + \frac{a_3}{4}\eta\eta' r \\ & + \left[\frac{C^{(1)}K_0{}' + K_1{}'}{16}\right](2\eta^2 r - r^3) + \left[\frac{C^{(1)}K_0 + K_1}{4}\right]\eta\eta' r, \end{aligned} \tag{45}$$

$$u_p^{(0)} = \frac{K_0}{4}\left(r^2 - \eta^2 - \frac{4}{M}\right) - 1, \tag{46}$$

$$v_p^{(0)} = \frac{K_0\eta\eta'}{4}r - \frac{K_0{}'}{16}\left(r^3 - 2\eta^2 r - \frac{8}{M}r\right), \tag{47}$$

$$K_1 = -\frac{a_1}{6}\eta^4 - \frac{a_2}{3}\eta^2 - a_3 + \frac{8C^{(1)}}{\pi}\left[\frac{q^{(0)} + \pi\eta^2}{\eta^6}\right]\left(\frac{8}{M} + \eta^2\right) - \frac{8q^{(1)}}{\pi\eta^4}. \tag{48}$$

The expressions for a_1 to a_3 are given in Appendix B.
The system Eqs. (33)–(38) is solved like the zeroth and first order. Note that the total flow rate for the second order is $q^{(2)} = q_f^{(2)} + q_p^{(2)}$, where $q_f^{(2)} = 2\pi \int_0^\eta u_f^{(2)} r \, \mathrm{d}r - 2\pi C^{(1)} \int_0^\eta u_f^{(1)} r \, \mathrm{d}r$ and $q_p^{(2)} = 2\pi C^{(1)} \int_0^\eta u_p^{(1)} r \, \mathrm{d}r$.
The solution at the second order is given by

$$\begin{aligned} u_f^{(2)} = {} & \frac{b_1}{100}\left(r^{10} - \eta^{10}\right) + \frac{b_2}{64}\left(r^8 - \eta^8\right) + \frac{b_3}{36}\left(r^6 - \eta^6\right) + \frac{b_4}{16}\left(r^4 - \eta^4\right) + \frac{b_5}{4}\left(r^2 - \eta^2\right) \\ & + \left[\frac{C^{(1)2}K_0 + C_0K_1 + K_2}{4}\right]\left(r^2 - \eta^2\right), \end{aligned} \tag{49}$$

$$\begin{aligned} v_f^{(2)} = {} & -\frac{b_1{}'}{1200}(r^{11} - 6\eta^{10} r) - \frac{b_2{}'}{640}(r^9 - 5\eta^8 r) - \frac{b_3{}'}{288}(r^7 - 4\eta^6 r) - \frac{b_4{}'}{96}(r^5 - 3\eta^4 r) - \frac{b_5{}'}{16}(r^3 - 2\eta^2 r) \\ & + \frac{b_1}{20}\eta^9\eta' r + \frac{b_2}{16}\eta^7\eta' r + \frac{b_3}{12}\eta^5\eta' r + \frac{b_4}{8}\eta^3\eta' r + \frac{b_5}{4}\eta\eta' r + \left[\frac{C^{(1)2}K_0{}' + C^{(1)}K_1{}' + K_2{}'}{16}\right](2\eta^2 r - r^3) \\ & + \left[\frac{C^{(1)2}K_0 + C^{(1)}K_1 + K_2}{4}\right]\eta\eta' r, \end{aligned} \tag{50}$$

$$
\begin{aligned}
u_p^{(1)} &= \frac{a_1}{36}\left(r^6-\eta^6\right)+\frac{a_2}{16}\left(r^4-\eta^4\right)+\frac{a_3}{4}\left(r^2-\eta^2\right)-\frac{\alpha Re_0 K_0 K_0{}'}{32M}\left(r^4+2\eta^4\right)\\
&+\frac{Re_0}{4}\left(\frac{\alpha K_0{}' K_0}{M^2}+\frac{\alpha K_0{}'}{M}\right)(r^2-\eta^2)+\frac{K_1}{4}\left(r^2-\eta^2\right)-\frac{\alpha Re_0 K_0 K_0{}'}{16M}\eta^2 r^2-\frac{\alpha Re_0 K_0{}^2}{8M}\eta^3\eta'-\frac{\alpha Re_0 K_0{}^2}{2M^2}\eta\eta'\\
&-\frac{\alpha Re_0 K_0}{2M}\eta\eta'-\frac{5C^{(1)}K_0}{2M}-\frac{K_1}{M}+\frac{C^{(1)}K_0}{4}r^2, \qquad (51)\\
v_p^{(1)} &= -\frac{a_1{}'}{288}\left(r^7-4\eta^6 r\right)-\frac{a_2{}'}{96}\left(r^5-3\eta^4 r\right)-\frac{a_3{}'}{16}\left(r^3-2\eta^2 r\right)+\frac{a_1}{12}\eta^5\eta' r+\frac{a_2}{8}\eta^3\eta' r+\frac{a_3}{4}\eta\eta' r\\
&+\left(\frac{\alpha Re_0(K_0{}')^2}{192M}+\frac{\alpha Re_0 K_0 K_0{}''}{192M}\right)\left(6\eta^4 r-3\eta^2 r^3-r^5\right)\\
&+\left(\frac{\alpha Re_0 K_0 K_0{}''}{16M^2}+\frac{\alpha Re_0 K_0{}''}{16M}+\frac{\alpha Re_0(K_0{}')^2}{16M^2}\right)\left(2\eta^2 r-r^3\right)+\left(\frac{\alpha Re_0 K_0{}'}{2M}+\frac{\alpha Re_0 K_0 K_0{}'}{M^2}+\frac{K_1}{4}\right)\eta\eta' r\\
&+\left(\frac{\alpha Re_0 K_0}{4M}+\frac{\alpha Re_0 K_0{}^2}{4M^2}\right)\eta\eta'' r+\left(\frac{\alpha Re_0 K_0{}^2}{4M^2}+\frac{\alpha Re_0 K_0}{4M}\right)(\eta')^2 r+\left(\frac{3\alpha Re_0 K_0{}^2}{16M}(\eta')^2+\frac{K_1{}'}{8}\right)\eta^2 r\\
&+\left(\frac{\alpha Re_0 K_0 K_0{}'\eta'}{4M}+\frac{\alpha Re_0 K_0{}^2\eta''}{16M}\right)\eta^3 r-\frac{\alpha Re_0 K_0 K_0{}'}{32M}\eta\eta' r^3-\frac{C^{(1)}K_0{}'}{16}r^3-\frac{K_1{}'}{16}r^3+\frac{\alpha Re_0 K_0 K_0{}''}{2M^3}r\\
&+\frac{\alpha Re_0(K_0{}')^2}{2M^3}r+\frac{K_1{}'}{2M}r+\frac{\alpha Re_0 K_0{}''}{2M^2}r+\frac{5C^{(1)}K_0{}'}{4M}r, \qquad (52)\\
K_2 &= -\frac{b_1}{15}\eta^8-\frac{b_2}{10}\eta^6-\frac{b_3}{6}\eta^4-\frac{b_4}{3}\eta^2-b_5+\frac{a_1}{6}C^{(1)}\eta^4+\frac{1}{3}\left(\frac{4a_1C^{(1)}}{M}+a_2C^{(1)}\right)\eta^2+\frac{a_3}{3}C^{(1)}+\frac{8a_2}{3M}C^{(1)}\\
&-\left(2C^{(1)2}-\frac{C^{(1)}a_3}{M}\right)\frac{8}{\eta^2}-\frac{16}{3}\frac{\alpha Re_0 C^{(1)}}{M}\frac{\eta'}{\eta^3}+\left(\frac{6\alpha Re_0 C^{(1)}q^{(0)}}{\pi M^2}+\frac{\alpha Re_0 C^{(1)}q^{(0)2}}{\pi^2 M}+\frac{16\alpha Re_0 C^{(1)}}{M^3}\right)\frac{64\,\eta'}{\eta^7}\\
&+\left(\frac{6\alpha Re_0 C^{(1)}q^{(0)}}{M^3}+\frac{\alpha Re_0 C^{(1)}q^{(0)2}}{\pi M^2}\right)\frac{512\,\eta'}{\pi\eta^9}+\left(\frac{C^{(1)2}q^{(0)}}{M}+\frac{2C^{(1)}q^{(1)}}{M}-\frac{16\pi C^{(1)2}}{M^2}\right)\frac{32}{\pi\eta^6}\\
&+\left(C^{(1)}q^{(1)}-2\,C^{(1)2}q^{(0)}-q^{(2)}+\frac{4\pi C^{(1)2}}{M}\right)\frac{8}{\pi\eta^4}+\frac{2048\alpha Re_0 C^{(1)}q^{(0)2}}{\pi^2 M^3}\frac{\eta'}{\eta^{11}}\\
&-\frac{512C^{(1)2}q^{(0)}}{\pi M^2\eta^8}. \qquad (53)
\end{aligned}
$$

The expressions for b_1 to b_5 are given in Appendix B.

B Expressions for *a*s and *b*s

$$
\begin{aligned}
a_1 &= \frac{Re_0}{32}K_0K_0{}',\\
a_2 &= -\frac{Re_0}{16}\left(K_0\eta^2+4\right)K_0{}',\\
a_3 &= \frac{Re_0}{16}\left(K_0\eta^2+4\right)\left(K_0{}'\eta+2K_0\eta'\right)\eta,\\
b_1 &= \frac{Re_0}{288}\left(\frac{3}{2}a_1{}'K_0-a_1K_0{}'\right),\\
b_2 &= \frac{Re_0}{144}\left(2a_1K_0{}'-a_1{}'K_0\right)\eta^2+\frac{Re_0}{36}a_1K_0\eta'\eta+\frac{Re_0}{96}a_2{}'K_0-\frac{Re_0}{36}a_1{}',\\
b_3 &= \frac{Re_0}{64}\left(a_2K_0{}'-a_2{}'K_0\right)\eta^2+\frac{Re_0}{32}a_2K_0\eta'\eta+\frac{Re_0}{64}\left(C^{(1)}K_0K_0{}'+2K_1{}'K_0+2a_3{}'K_0+2\alpha C^{(1)}K_0{}'K_0\right)\\
&+\frac{Re_0}{32}K_0{}'K_1+\frac{Re_0}{32}\left(a_3K_0{}'-2a_2{}'\right),
\end{aligned}
$$

$$
\begin{aligned}
b_4 = & -\frac{Re_0}{144}a_1{K_0}'\eta^6 - \frac{Re_0}{64}a_2{K_0}'\eta^4 - \frac{Re_0}{32}\left((C^{(1)}{K_0}' + 2{K_1}' + 2{a_3}' + 2\alpha C^{(1)}{K_0}')K_0 + 2{K_0}'K_1 + 2a_3{K_0}'\right)\eta^2, \\
& - \frac{Re_0}{4M}\alpha C^{(1)}{K_0}'K_0 - \frac{Re_0}{8}\left(2{K_1}' - C^{(1)}{K_0}' + 2\alpha C^{(1)}{K_0}' + 2{a_3}'\right), \\
b_5 = & \frac{Re_0}{144}\left(a_1{K_0}' + {a_1}'K_0\right)\eta^8 + \frac{Re_0}{18}a_1K_0\eta'\eta^7 + Re_0\left(\frac{{a_2}'K_0}{64} + \frac{1}{576}\left(9a_2{K_0}' + 16{a_1}'\right)\right)\eta^6 \\
& + Re_0\left(\frac{3}{32}a_2K_0\eta' + \frac{a_1}{6}\eta'\right)\eta^5 + \frac{Re_0}{32}\left(C^{(1)}{K_0}' + 2{K_1}' + 2{a_3}' + 2\alpha C^{(1)}{K_0}'\right)K_0\eta^4 + \frac{Re_0}{16}{K_0}'K_1\eta^4 \\
& + \frac{Re_0}{16}\left({a_2}' + a_3{K_0}'\right)\eta^4 + \frac{Re_0}{16}C^{(1)}\eta'(2\alpha+1){K_0}^2\eta^3 + \frac{Re_0}{4}\left(K_1\eta' + a_3\eta'\right)K_0\eta^3 + \frac{Re_0}{4}a_2\eta'\eta^3 \\
& + \frac{Re_0}{2M}\alpha C^{(1)}{K_0}'K_0\eta^2 + \frac{Re_0}{8}\left(2{K_1}' - C^{(1)}{K_0}' + 2\alpha C^{(1)}{K_0}' + 2{a_3}'\right)\eta^2 + \frac{Re_0}{2M}C^{(1)}\alpha\eta'{K_0}^2\eta \\
& + \frac{Re_0}{4}C^{(1)}(2\alpha-1)K_0\eta'\eta + \frac{Re_0}{2}K_1\eta'\eta + \frac{Re_0}{2}a_3\eta'\eta + \frac{Re_0}{M^2}\alpha C^{(1)}{K_0}'K_0 + \frac{Re_0}{M}C^{(1)}{K_0}'.
\end{aligned}
$$

The primes denote differentiation with respect to z.

References

1. Shapiro, A.H., Jaffrin, M.Y., Weinberg, S.L.: Peristaltic pumping with long wavelengths at low Reynolds number. J. Fluid Mech. **37**, 799–825 (1969)
2. Yin, F., Fung, Y.C.: Peristaltic transport. J. Appl. Mech. **35**, 669–675 (1969)
3. Zien, T.F., Ostrach, S.: A long wave approximation of peristaltic motion. J. Biomech. **3**, 63–75 (1970)
4. Manton, M.J.: Long-wavelength peristaltic pumping at low Reynolds number. J. Fluid Mech. **68**, 681–693 (1975)
5. Lykoudis, P., Roos, R.: The fluid mechanics of the ureter from a lubrication theory point of view. J. Fluid Mech. **43**, 661–674 (1970)
6. Griffiths, D.J.: Flow of urine through the ureter: a collapsible, muscular tube undergoing peristalsis. J. Biomech. Eng. **111**, 206–211 (1989)
7. Takabatake, S., Ayukawa, K., Mori, A.: Peristaltic flow in circular cylindrical tubes under finite wavelengths and finite Re. J. Fluid Mech. **193**, 267–283 (1988)
8. Xiao, Q., Damodaran, M.: A numerical investigation of peristaltic waves in circular tubes. Int. J. Comput. Fluid Dyn. **16**(3), 201–216 (2002)
9. Yin, F., Fung, Y.: Comparison of theory and experiment in peristaltic transport. J. Fluid Mech. **47**, 93–112 (1971)
10. Ramachandra Rao, A., Mishra, M.: Nonlinear and curvature effects on peristaltic flow of a viscous fluid in an asymmetric channel. Acta Mech. **168**, 35–59 (2001)
11. Srinivasacharya, W., Mishra, M., Rao, A.R.: Peristaltic pumping of a micropolar fluid in a tube. Acta Mech. **161**, 165–178 (2003)
12. Hayat, T., Ali, N., Ashgar, A.: An analysis of peristaltic transport for flow of a Jeffrey fluid. Acta Mech. **193**, 101–112 (1998)
13. Pozrikidis, C.: A study of peristaltic flow. J. Fluid Mech. **180**, 515–527 (1987)
14. Graw, M., Engelhardt, H.: Simulation of physiological ureteral peristalsis. Urol. Int. **41**, 1–8 (1986)
15. Misra, J.C.: Biomathematics: Modelling and Simulation. World Scientific, Singapore (2006)
16. Misra, J.C., Pandey, K.: A mathematical model for oesophageal swallowing of a food-bolus. Math. Comput. Model. **33**, 997–1009 (2001)
17. Widmaier, E.P., Raff, H., Strang, K.T.: Vander's Human Physiology: The Mechanisms of Body Function. McGraw-Hill, New York (2001)
18. Mernone, A.V., Mazumdar, J.N., Lucas, S.K.: A mathematical study of peristaltic transport of a Casson fluid. Math. Comput. Model. **35**, 895–912 (2002)
19. Misra, J., Pandey, K.: Peristaltic transport of blood in small vessels: study of a mathematical model. Comput. Math. Appl. **43**, 1183–1193 (2002)
20. Gupta, B.B., Seshadri, V.: Peristaltic transport in non-uniform tubes. J. Biomech. **9**, 105–109 (1976)
21. Fauci, L.J., Dillon, R.: Biofluidmechanics of reproduction. Annu. Rev. Fluid Mech. **38**, 371–394 (2006)
22. Eytan, O., Elad, D.: Analysis of intra-uterine fluid motion induced by uterine contractions. Bull. Math. Biol. **61**, 221–238 (1999)
23. Ishii, M., Hibiki, T.: Thermo-Fluid Dynamics of Two-Phase Flow. Springer, Berlin (2006)
24. Drew, D.: Stability of a Stokes layer of a dusty gas. Phys. Fluids **22**(11), 2081–2086 (1979)
25. Drew, D.: Mathematical modeling of two-phase flow. Annu. Rev. Fluid Mech. **15**, 261–291 (1983)
26. Drew, D.A., Passman, S.L.: Theory of Multicomponent Fluids. Springer, Berlin (1999)
27. Kleinstreuer, C.: Two-Phase Flow: Theory and Applications. Taylor and Francis, London (2003)
28. Enwald, H., Peirano, E., Almstedt, A.E.: Eulerian two-phase flow theory applied to fluidization. Int. J. Multiph. Flow **22**, 21–66 (1996)
29. Patankar, N.A., Joseph, D.D.: Modeling and numerical simulation of particulate flows by the Eulerian–Lagrangian approach. Int. J. Multiph. Flow **27**, 1659–1684 (2001)

30. Jiménez-Lozano, J., Sen, M., Dunn, P.F.: Particle motion in unsteady two-dimensional peristaltic flow with application to the ureter. Phys. Rev. E **79**(4), 041901 (2009)
31. Jiménez-Lozano, J., Sen, M.: Particle dispersion in two-dimensional peristaltic flow. Phys. Fluids **22**, 043303 (2010)
32. Stewart, H.B.: Two-phase flow: models and methods. J. Comput. Phys. **56**, 363–409 (1984)
33. Srivastava, L.M., Srivastava, V.P.: Peristaltic transport of a particle-fluid suspension. J. Biomech. Eng. **111**, 157–165 (1989)
34. Mekheimer, K.S., El Shehawey, E.F., Elaw, A.M.: Peristaltic motion of a particle-fluid suspension in a planar channel. Int. J. Theor. Phys. **37**(11), 2895–2920 (1998)
35. Misra, J., Pandey, K.: Peristaltic transport of particle-fluid suspension in a cylindrical tube. Comput. Math. Appl. **28**(4), 131–145 (1994)
36. Sha, W.T., Soo, S.L.: On the effect of $P\nabla\alpha$ term in multiphase dynamics. Int. J. Multiph. Flow **5**, 153–158 (1979)
37. Felderhof, B.U.: Virtual mass and drag in two-phase flow. J. Fluid Mech. **225**, 177–196 (1991)
38. Drew, D.A.: Two-phase flows: constitutive equations for lift and Brownian motion and some basic flows. Arch. Ration. Mech. Anal. **62**(2), 149–163 (1976)
39. Charm, S., Kurland, G.: Blood Flow and Microcirculation. Wiley, New York (1974)
40. Siddiqui, A.M., Schwarz, W.H.: Peristaltic flow of a second-order fluid in tubes. J. Non-Newton. Fluid Mech. **53**, 257–284 (1994)
41. Boyarski, S., Gottschalk, C., Tanagho, E., Zimskind, P.: Urodynamics: Hydrodynamics of the Ureter and Renal Pelvis. Academic Press, San Diego (1971)
42. Guerra, A., Allegri, F., Meschi, T., Adorni, G., Prati, B., Nouvenne, A., Novarini, A., Maggiore, U., Fiaccadori, E., Borghi, L.: Effects of urine dilution on quantity, size and aggregation of calcium oxalate crystals induced in vitro by an oxalate load. Clin. Chem. Lab. Med. **43**(6), 585–589 (2005)
43. Jiménez-Lozano, J., Sen, M.: Streamline topologies of two-dimensional peristaltic flow and their bifurcations. Chem. Eng. Process. Process Identif. **49**(7), 704–715 (2010)
44. Shigeta, M., Kasaoka, Y., Yasumoto, H., Inoue, K., Usui, T., Hayashi, M., Tazuma, S.: Fate of residual fragments after successful extracorporeal shock wave lithotripsy. Int. J. Urol. **6**, 169–172 (1999)
45. Kiil, F.: The Function of the Ureter and Renal Pelvis. W.B. Saunders, Philadelphia (1957)
46. Boyarski, S., Labay, P.: Ureteral Dynamics. The Williams and Wilkins Co., Baltimore (1972)
47. Weinberg, S.L.: Ureteral function: II. The ureteral catheter and the uremetrogram. Investig. Urol. **12**(4), 255–261 (1975)
48. Shafik, A.: Electroureterogram: human study of the electromechanical activity of the ureter. Urology **48**(5), 696–699 (1996)
49. Shafik, A.: Ureteric profilometry: a study of the ureteric pressure profile in the normal and pathologic ureter. Scand. J. Urol. Nephrol. **32**, 14–19 (1997)